Heterogeneity of Epidermal Growth Factor Binding Kinetics on Individual Cells

Johnson C. Chung, Noah Sciaky, and David J. Gross
Department of Biochemistry and Molecular Biology and Program in Molecular and Cellular Biology, University of Massachusetts, Amherst, Massachusetts 01003-4505 USA

ABSTRACT Binding of fluorescein-conjugated epidermal growth factor (EGF) to individual A431 cells at 4°C is measured by a quantitative fluorescence imaging technique. After background fluorescence and cell autofluorescence photobleaching corrections, the kinetic data are fit to simple models of one monovalent site and two independent monovalent sites, both of which include a first-order dye photobleaching process. Model simulations and the results from data analysis indicate that the one-monovalent-site model does not describe EGF binding kinetics at the single-cell level, whereas the two-site model is consistent with, but not proved by, the single-cell binding data. In addition, the kinetics of binding of fluorescein-EGF to different cells from the same coverslip often differ significantly from each other, indicating cell-to-cell variations in the binding properties of the EGF receptor.

INTRODUCTION

Epidermal growth factor (EGF), of either mouse or human origin, in its fully processed form is a single polypeptide of 53 amino acids with three intramolecular disulfide bonds and no glycosylation (Savage et al., 1972; Taylor et al., 1972). It binds to the EGF receptor (EGFR) at the cell surface initially to induce ion fluxes and cell morphology changes, such as membrane ruffling, and subsequently cell proliferation in epithelial and several other cell types (Carpenter and Cohen, 1979, 1981; Chinkers et al., 1979, 1981). The EGFR is a single glycoprotein with one putative transmembrane segment and a molecular mass of ~170 kDa (Ullrich et al., 1984). Its extracellular portion contains the amino terminus and has 622 amino acids with approximately 12 N-linked glycosylation sites (Cummings et al., 1985; Mayes and Waterfield, 1984; Slieker and Lane, 1985; Ullrich et al., 1984). Furthermore, this region is organized into four domains, two of which are cysteine-rich; together, the four domains form the binding pocket for EGF, with the intervening non-cysteine-rich domain contributing the most to EGF binding (Lax et al., 1988, 1989; Ullrich et al., 1984). The putative transmembrane segment is 23 amino acids in length and has a high hydrophobic content (Ullrich et al., 1984). The cytoplasmic domain has 542 amino acids and contains five tyrosine phosphorylation SH2 domain-binding sites, seven serine/threonine phosphorylation sites, an actin-binding site overlapping the Y992 phosphorylation site, one domain required for receptor internalization, one protein tyrosine kinase (PTK) region, and the carboxyl terminus (Boonstra et al., 1995; Carpenter and Cohen, 1990; Ullrich et al., 1984). EGF-bound receptors cluster at coated pits and are subsequently internalized and degraded or partially recycled under normal physiological conditions (Haigler et al., 1978, 1979; Masui et al., 1993; McKanna et al., 1979).

Scatchard plots of equilibrium EGF binding to several cell types, expressing either native or transfected EGFR, have all shown a curvilinear appearance characteristic of negative cooperativity (referred to as "negative curvature" henceforth; Bellot et al., 1990; Defize et al., 1989). It has been shown that only a single cDNA sequence of EGFR is required to produce such negative curvature in Scatchard plots from a population of receptor-null cells that were transfected with the WT EGFR (Bellot et al., 1990; Davis et al., 1988; Schlessinger, 1986). Given the 1:1 molar ratio of bound EGF to EGFR reported by Weber, Bertics, and Gill (Weber et al., 1984a), these curvilinear Scatchard plots are generally interpreted to mean that two receptor affinity classes exist in the experimental systems (Carpenter, 1987; Schlessinger, 1988).

However, the source of the observed receptor heterogeneity is not known in such experiments. For example, it is not clear that the observed receptor heterogeneity is indeed from each cell rather than being the result of population diversity. Such heterogeneity in binding affinity could be the result of different posttranslational modifications of receptors on different subpopulations of cells. The negative curvature could also be caused by variable receptor density on cells or isolated membrane vesicles within a population if EGF binding is diffusion-limited and therefore influenced by receptor density. Variable receptor density can result from different cell sizes, different stages in cell growth, or simply a different receptor expression level. It is difficult to exclude all of these possibilities based on population equilibrium binding experiments. These ambiguities are clari-

Received for publication 20 November 1996 and in final form 17 April 1997.

Address reprint requests to Dr. David J. Gross, Department of Biochemistry and Molecular Biology, Lederle GRC, University of Massachusetts, Box 34505, Amherst, MA 01003-4505. Tel.: 413-545-3170; Fax: 413-545-3291; E-mail: dgross@chemserv.chem.umass.edu.

Dr. Chung's present address is Department of Biochemistry, Brandeis University, Waltham, MA, 02254.

Dr. Sciaky's present address is National Jewish Center for Immunology and Respiratory Medicine, 1400 Jackson Street, Denver, CO 80206.

0006-3495/97/08/1089/14 $2.00

fied by studying ligand-receptor binding kinetics at the single-cell level.

Experiments with monoclonal antibodies that block either the high-affinity (Bellot et al., 1990) or the low-affinity (Gregoriou and Rees, 1984; Defize et al., 1989) states of the EGFR suggest that these two affinity states are conformationally distinguishable at the extracellular domain of the receptor. Preincubation of A431 cell monolayers with either mAb EGR/G49 (Gregoriou and Rees, 1984) or mAb 2E9 (Defize et al., 1989) show that the negative-curvature Scatchard plots characteristic of EGF binding to A431 cells are converted to straight-line Scatchard plots corresponding to high-affinity binding of EGF. Double immunofluorescence labeling of A431 cells by mAb EGR/G49 suggests that all A431 cells bind this antibody (Gregoriou and Rees, 1984). Prebinding of A431 cells with mAb 2E9 followed by incubation with fluorescein-labeled EGF and rhodamine-labeled or unlabeled EGF at 50 nM total concentration shows that ~80% of control levels of EGF binding is lost on all cells (Gadella and Jovin, 1995). These results suggest that the heterogeneity of EGFR ligand binding affinity states is present at the individual cell level, although there may be alternative explanations. As an example, in the latter study, incomplete block by mAb 2E9, either by steric restrictions on antibody access or by antibody debinding, could have left a population of low-affinity EGFR accessible to EGF on any particular cell, thus allowing fluorescent ligand binding on all cells, some of which could have been expressing only one affinity class of receptor. Also possible with such mAb binding experiments is the conversion by antibody-EGFR interaction of the distribution of EGFR states on individual cells. Thus it seems appropriate to employ direct ligand binding to individual cells to determine if the heterogeneity of EGF binding states is present at the single-cell level. The results presented below are consistent with the above-cited references in that two kinetically distinguishable EGF binding states are seen on individual cells.

The A431 cell line (Giard et al., 1973) was selected as the in vivo experimental system for this study, and quantitative fluorescence imaging as the data acquisition method. These cells express a large number of EGFR at the cell surface, $\sim 2 \times 10^6$ receptors per cell, which is ~10–15 times the receptor density expressed in most normal cells (Fabricant et al., 1977; Haigler et al., 1978; Wrann and Fox, 1979). The abnormally high receptor density is attributed to gene amplification by chromosome translocation and rearrangement, resulting in multiple copies of the receptor gene and a truncated version of the gene (Shimizu and Kondo, 1982; Ullrich et al., 1984). In addition to the glycosylated, functional receptors expressed at the cell surface, A431 cells also secrete a soluble, glycosylated, truncated version of the receptor containing only the extracellular domain of the receptor, most likely the product of the truncated gene (Ullrich et al., 1984; Weber et al., 1984b). Although the high receptor density on A431 cells enhances the signal-to-noise ratio for signal detection in kinetics experiments, which makes this cell line a test system, it also complicates analysis of binding kinetics because of the possible involvement of diffusion-limited binding, which has been reported in A431 cells as studied in populations (Berkers et al., 1992; Wiley, 1988). Nevertheless, Scatchard plots obtained from EGF binding to a population of A431 cells show the characteristic negative curvature seen in other cell types (van Bergen en Henegouwen et al., 1989).

We report herein the kinetics of fluorescein-conjugated EGF (f-EGF) binding to individual A431 cells recorded with a quantitative fluorescence imaging technique. The kinetic data are fitted to simple models of one monovalent site and two independent monovalent sites, both with the addition of a first-order dye photobleaching process, and are compared to simulated data obtained with kinetic constants reported in the literature. Kinetics of EGF/EGFR binding at the single cell level do not follow a simple one-monovalent-site model and show significant variations from cell to cell.

MATERIALS AND METHODS

Fluorescent probe

f-EGF (Molecular Probes, Eugene, OR) was used for the experiments. The equilibrium binding of f-EGF to cells has been shown to be identical to that of EGF by an equilibrium competition assay (Carraway and Cerione, 1991; Chatelier et al., 1986; Gadella and Jovin, 1995); thus, by extension, the kinetics of binding of f-EGF are assumed to be identical to that of EGF.

A431 cells

A431 cells used for all experiments were purchased from the American Type Culture Collection (Rockville, MD) and propagated in Dulbecco's modified Eagle's medium (Gibco BRL, Grand Island, NY) supplemented with 5% fetal calf serum (HyClone, Logan, UT) without antibiotic treatment. Cells were plated on no. 1 glass coverslips for imaging experiments. Approximately 5×10^4 cells were plated drop by drop onto different locations of each glass coverslip (Fisher, Pittsburgh, PA). The cells were serum-starved 2 days after plating; imaging experiments on the cells were carried out 3 days after plating, allowing at least overnight serum starvation before each experiment. Cells were transferred to HEPES-buffered saline (HBS) (10 mM HEPES, 140 mM NaCl, 5 mM KCl, 1 mM $CaCl_2$, 1 mM $MgCl_2$, and 10 mM α-D-glucose, titrated to pH 7.4 and sterile filtered), containing 0.1% (1 mg/ml) bovine serum albumin (BSA) (Sigma), just before imaging experiments. Receptor internalization is negligible at 4°C, the temperature at which all data are collected; this is based on published results demonstrating the temperature dependence of endocytosis for A431 cells and two other mammalian cell types (Haigler et al., 1979; Tomoda et al., 1989; Weigel and Oka, 1981), as well as the lack of incorporation into cells, as judged by optical microscopy, of f-EGF in experiments here.

Imaging system

Quantitative fluorescence imaging microscopy was used for data acquisition (Linderman et al., 1990). A Zeiss IM 35 inverted microscope equipped with a Nikon fluor 40/1.30 oil objective was used for epifluorescence microscopy. In addition, both the sample stage and the objective were temperature-controlled (4°C). A 470-nm bandpass filter (470DF10; Omega, Brattleboro, VT) was used to select the excitation light from an ultrastable mercury-xenon arc lamp (L2422 100 W; Hamamatsu Photonics, Japan). A 510-nm long-pass dichroic mirror (FT510; Zeiss, Thornwood, NY) in combination with a 530-nm bandpass second barrier filter (530DF30; Omega) were used for signal filtering. A slow-scan charge-coupled device (CCD) camera (a Thomson CSF TH 7882 CCD housed in

a CH250 camera head; Photometrics, Tucson, AZ) was used for signal recording. A computer-controlled shutter was placed in front of the arc lamp to allow periodic excitation of the samples (Fig. 1). In general, images were collected such that 16 image pixels in 4 × 4 arrays on the CCD were combined into superpixels of 2.1 × 2.1 μm dimension on the cell surface. Specific regions of interest were defined interactively by selecting all image pixels within a user-defined area from one digital image of a sequence and used to obtain the average pixel value of the same region from all images in an experiment. No corrections for uneven illumination of the samples and uneven detection by the CDD were applied, because such variations over the dimension of a single cell were small.

Imaging protocol

The following steps were followed for a typical f-EGF binding and debinding experiment performed at 4°C. Cells plated on a coverslip were loaded into a culture chamber that permits solution exchange (Linderman et al., 1990), placed on the microscope stage, and brought to focus using transmitted light imaging. Binding data acquisition was initiated after the cells were subjected to 1 min of fluorescence excitation light. Preliminary experiments showed that A431 cell autofluorescence photobleached at two distinct rates. Given the fluorescence excitation level of the microscope system used in these studies, the faster photobleaching phase was found to be complete within 1 min (data not shown). After the initial 1 min of photobleaching, the residual cellular autofluorescence decayed at a much slower rate, and thus photobleaching was incomplete over the time courses used in these experiments (Fig. 2). The amplitude of the bleachable autofluorescence in A431 cells was rather small and variable between cells as determined in separate experiments; the example in Fig. 2 is one of the better traces. The quantitative measurement of this autofluorescence decay was found to be difficult because of the dimness of A431 cell images after the 1-min prebleaching period—in particular, identification of individual cells and confirmation that they did not move over the course of an experiment were difficult to achieve. Autofluorescence photobleaching fluorescence decay from two cells that appeared to have been properly measured, fit to a single exponential function with an offset, i.e. a component of the A431 cell autofluorescence was not bleachable under the conditions used here. The measured amplitude of the decaying phase of the autofluorescence was found to be 4.4 ± 0.3 fluorescence units and the rate constant to be 0.0054 ± 0.0005 min^{-1}. Over the longest times of f-EGF binding in experiments reported here, autofluorescence decay then amounts to only ~1.5 fluorescence units, or a few percent at most of any imaging data values. As discussed below, a correction for autofluorescence photobleaching was applied to all cell data sets.

In each experiment, a few images of the cells were taken before the addition of the fluorescein calibration solution (3.3×10^{-6} mg/ml fluorescein in HBS) was added to the chamber; fluorescein solution addition allowed calibration of cell region background f-EGF fluorescence relative to a noncell background f-EGF fluorescence by measuring the relative fluorescence of the two regions in fluorescein solution before the actual binding experiment was initiated (see the section on data treatment). The fluorescein solution was washed away with HBS after a few images had been taken. After that, solution containing f-EGF was added to start the binding phase of the experiment; it generally lasted 80 min. After binding,

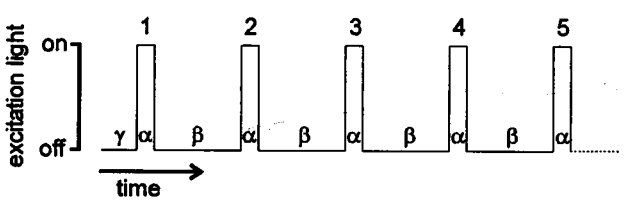

FIGURE 1 Periodic excitation scheme. γ = initial delay time from ligand addition to first exposure. α = exposure time. β = time between excitation light pulses. Five pulses are shown, as numbered in the figure.

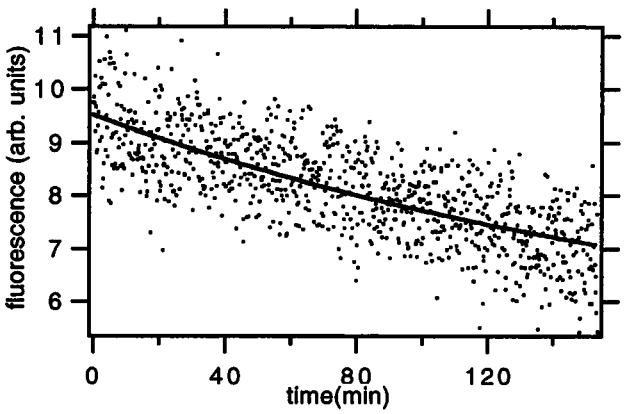

FIGURE 2 Autofluorescence photobleaching of A431 cells. Each data point is from an image of a cell exposed to excitation light for 250 ms; such images were recorded approximately every 10 s. EGF (17 nM) was added at time 0. The data were fit to a single exponential function plus a constant, shown by the solid line.

free f-EGF was washed away from the chamber. The ensuing debinding phase of the experiment was generally monitored for ~70 min. Images were taken approximately every 10 s throughout the experiment. Periodic renewal of f-EGF solution was not necessary because the free f-EGF supply was not diminished noticeably during binding experiments (see Fig. 3). Each solution exchange step consists of two separate solution additions of at least 1.8 ml each to ensure better than 96% solution exchange (Cheyette and Gross, 1991).

Data treatment

The algorithm for background fluorescence correction and autofluorescence photobleaching correction is described below. For the binding phase of an experiment, base fluorescence levels, determined from images taken before the addition of either fluorescein solution or f-EGF solution, were subtracted from subsequent image data to give the cell (F_{cell}) and noncell ($F_{noncell}$) fluorescence signals. The values of F_{cell} thus represent the fluorescence detected from the cell less that due to the initial autofluorescence levels, both bleachable and unbleachable. The ratio $F_{cell}/F_{noncell}$ was av-

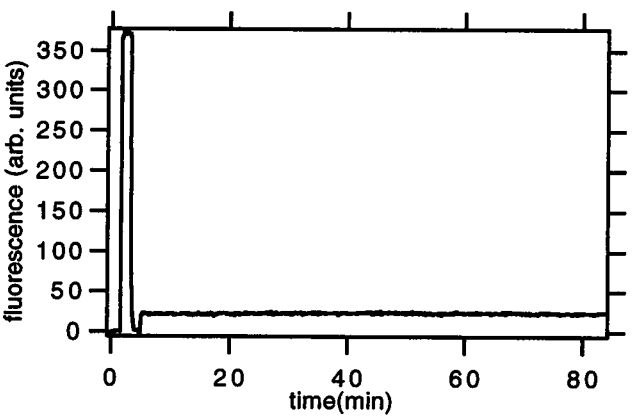

FIGURE 3 Fluorescence from a non-cell region during an experiment. The sequence of solution exchange in the cell chamber was as follows: fluorescein solution addition at ~1.5 min, dye-free solution wash at ~3.3 min, and 2.5 nM f-EGF solution addition at ~5 min. Each data point is from a ~10 × ~10 μm region of solution exposed periodically for 500 ms to excitation light and recorded approximately every 10 s.

eraged for the free fluorescein segment of the data and designated R_f. The cell volume and background fluorescence-corrected fluorescence signal (F) for subsequent f-EGF images was then obtained by

$$F = F_{cell} - (F_{noncell} \times R_f) \quad (1)$$

where F, F_{cell}, and $F_{noncell}$ are f-EGF fluorescence intensities. The fluorescence signal was further corrected for cell autofluorescence photobleaching by (see above for detail)

$$F = F + 4.4(1 - e^{-0.0054t}) \quad (2)$$

where t is the time in minutes. The maximum correction applied for the longest experiments described here, 1.5 fluorescence units, occurs at times for which f-EGF fluorescence is largest in binding experiments. Given the difficulty of obtaining individual cell autofluorescence decay data, the use of this approximation for autofluorescence decay seems justified.

For the debinding phase of an experiment, base fluorescence levels, also determined from images taken before the addition of either fluorescein solution or f-EGF solution, were subtracted from the cell (F_{cell}) and noncell ($F_{noncell}$) fluorescence signals. No cell volume correction was necessary in the absence of free f-EGF; therefore, the background-corrected fluorescence signal was computed as

$$F = F_{cell} - F_{noncell} \quad (3)$$

The method of correcting the fluorescence signal for cell autofluorescence photobleaching was similar to that used for the binding phase of the experiment, except that the initial autofluorescence level was calculated by incorporating the total binding time into the equation

$$F = F + 4.4(1 - e^{-0.0054(t+b)}) \quad (4)$$

where b is the duration of the binding experiment in minutes.

RESULTS

Controls

The bulk solution f-EGF was a constant source of nonbleached f-EGF in the experimental system. This was demonstrated by measuring the fluorescence of a noncell region of a field throughout an experiment; a typical measurement is shown in Fig. 3. The first peak in the figure shows the fluorescein calibration peak. The long-lasting, lower-amplitude fluorescence plateau represents the solution f-EGF fluorescence after the removal of free fluorescein from and the subsequent addition of f-EGF to the cell chamber. This fluorescence level stayed constant throughout, demonstrating that the source of nonbleached f-EGF was not depleted during an experiment.

A431 autofluorescence photobleaching over a 150-min period is approximated by a single exponential decay function with an amplitude of 4.4 fluorescence units and a decay rate of 0.0054 min^{-1}, as shown in Fig. 2. The data were obtained the same way as in the f-EGF binding experiments, except that 17 nM unlabeled EGF was used instead of f-EGF. As in regular experiments, the cells were first bleached by a continuous exposure to the excitation light for 1 min just before data acquisition; this step removed the fast autofluorescence photobleaching component from the bleaching curve and thus allowed the single exponential decay approximation. The single exponential decay curve is subsequently added back to the background-corrected data (see Data Treatment in Materials and Methods). Small variations in illumination intensity across the image were not corrected by this approximation.

Possible contributions to fluorescence changes over time caused by cell movement and morphology changes were eliminated by analyzing only data from cell regions showing little or no such behavior. Two images, one near the beginning of and another near the end of a binding experiment, were used to define two regions of interest from the same cell region; thus two sets of data were generated from the same cell region. Data sets were further analyzed only if the two sets of data were coincident, illustrated by the overlapping of circles and ×'s in Fig. 4.

Nonspecific binding of f-EGF to the coverslip or cell surface was negligible in our signal detection system. Chinese hamster ovary (CHO K1) cells, which do not express EGFR, were used as controls for cell membrane f-EGF nonspecific binding because there are no available EGFR-null A431 cells. The fluorescence intensities from noncell and cell regions showed no increase in absolute fluorescence after the addition of f-EGF, as shown in Fig. 5. This indicates that any nonspecific f-EGF binding to the cells or to the coverslip is either minimal or so slow as to be undetectable by our imaging system.

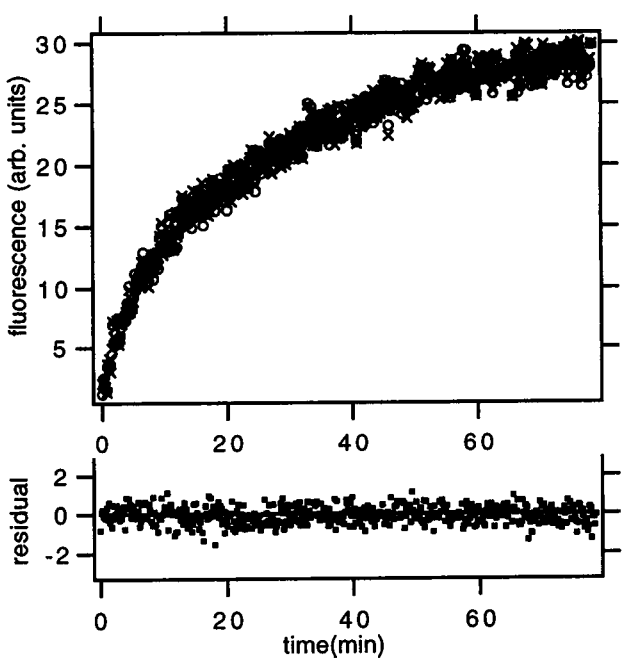

FIGURE 4 Test for fluorescence change due to cell movement and morphology change over time. Comparison of fluorescence intensities extracted from two cell image templates, both of the same cell region, with one template obtained from near the beginning of and another from near the end of a series of images, shows good agreement, as illustrated by the residual plot (■, *bottom plot*) and the overlap of the two data sets (○, ×, *top plot*). The residual is defined as the arithmetic difference between the two data sets.

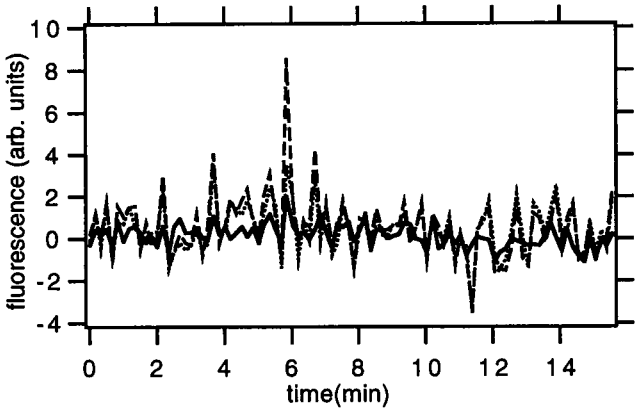

FIGURE 5 Nonspecific binding of f-EGF to the coverslip and CHO cells. An HBS solution containing 6.15 nM f-EGF and 0.1% bovine serum albumin was added to CHO cells at time 0 of the plot; the free fluorescein calibration peak and background fluorescence before the addition of f-EGF are not shown in this figure. Data from three regions, including one noncell region (——) and two cell regions (– – – and ·····), of the coverslip are shown. There is no increase in fluorescence in any of the regions over time. Each data point is from an image exposed for 250 ms; images were recorded approximately every 10 s.

f-EGF photobleaching correction

Receptor-bound f-EGF was photobleached significantly over the course of a typical imaging experiment. The effect of photobleaching on the fluorescence signal was demonstrated qualitatively by the changes in slopes between segments of data shown in Fig. 6. In these traces the continuous increase in bound f-EGF is shown to include a second kinetic process that reduces the rate of increase of f-EGF binding to the cell. This is interpreted as evidence for significant cell-surface f-EGF photobleaching during the experiment. Each steplike transition in the figure is due to a change in excitation light exposure time during one continuous binding experiment; the time between frames was kept the same (10 s) for the duration of the experiment. As expected, the average integrated fluorescence signal level during a segment increased with increasing exposure time; however, rates of fluorescence change were different for segments with different exposure times. These different slopes indicate different photobleaching rates for different exposure times, i.e. the longer the exposure time, the faster the photobleaching rate and shallower or more negative the slope. This was a photobleaching effect, because the ligand-receptor binding process itself was independent of the exposure scheme. This photobleaching effect was not negligible under most experimental conditions and was accounted for by incorporating a ligand photobleaching step, as shown below, into the models used for data analysis. In related experiments (not shown), the photobleaching rate was shown to be proportional to excitation light intensity, as one would expect for a simple photobleaching process. Thus photobleaching is a function of both exposure time and intensity of illumination. All experiments reported here were done with fixed fluorescence illumination intensity.

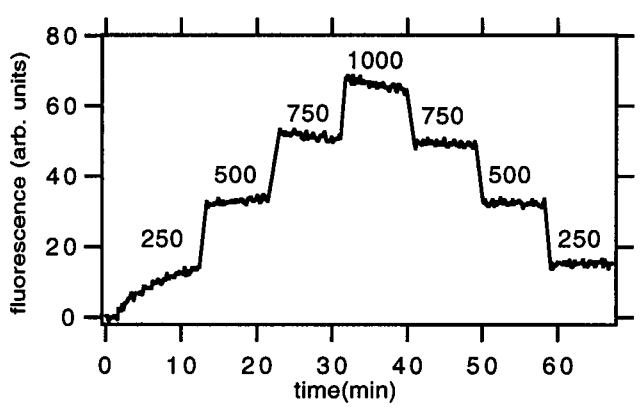

FIGURE 6 The effect of photobleaching on the fluorescence signal. Data were collected approximately every 10 s. After f-EGF addition (arrow), 250-, 500-, 750-, 1000-, 750-, 500-, and 250-ms exposure times were employed, respectively, during each data segment for data acquisition. The change in the f-EGF signal is due to ligand binding, differences in exposure time, and the degree of photobleaching of the bound f-EGF. These factors account for the differences in the level and rate of change of detected fluorescence from the cell.

A simple one-monovalent-site model was modified according to the periodic excitation protocol (Fig. 1) to account for f-EGF photobleaching. This modified model (shown below) included f-EGF (L) binding to the EGFR (R) with forward and reverse rate constants k_f and k_r and photobleaching of receptor-bound f-EGF (LR) with characteristic rate k_p:

$$\begin{array}{ccc} & \overset{k_f}{\rightleftarrows} & \\ L + R & & LR \\ & \underset{k_r}{} & \downarrow k_p \\ & \overset{k_f}{\rightleftarrows} & \\ L^* + R & & L^*R \\ & \underset{k_r}{} & \end{array}$$

Photobleached f-EGF is indicated with an asterisk; it no longer contributes to the fluorescence signal. During time γ before the cells were exposed to excitation light, only the top reaction occurred (i.e., no photobleaching). During time α, the entire reaction scheme was valid and photobleached f-EGF (L* and L*R) accumulated. The amounts of free photobleached f-EGF, L*, are vanishingly small for the duration of all experiments described here, because dissociation of L* from the cell surface is into 0.8 ml of cell buffer, effectively an infinite volume. During time β, the photobleaching excitation light was removed, i.e., k_p no longer connected the two top and bottom binding processes in the model; thus the kinetics during β were again described by simple monovalent ligand-receptor binding. In this model photobleached f-EGF that debinds from a receptor is assumed to be lost in the bulk buffer solution. Using the above reasoning, the time course of ligand binding during all segments (γ, α, and β) of an experiment was solved iteratively. The variable t (time) in each segment was defined only for the duration of the segment, i.e., the start of each segment is defined as $t = 0$, and the end of the segment

as t = duration of the segment. The detected signal, S_n, collected by the CCD camera during the excitation period n was the time integral of the fluorescence signal during the excitation pulse. The final equation for the measured signal S_n has the following form (see appendix for details):

$$S_n = Q \int_0^{\alpha} [\mathrm{LR}]_n \, dt \tag{5}$$

where Q is a scaling factor, $[\mathrm{LR}]_n = [\mathrm{LR}]$ during excitation period n, and

$$\int_0^{\alpha} [\mathrm{LR}]_n \, dt = \left(\frac{b_n}{\mathbf{k}} - \frac{L_T R_T k_f k_r}{\mathbf{k}^2 k}\right)(1 - e^{-\mathbf{k}\alpha}) + \frac{L_T R_T k_f k_r}{\mathbf{k}k}\alpha + \frac{L_T^2 R_T k_f^2}{k(\mathbf{k} - k)}\left(\frac{1}{k}(1 - e^{-k\alpha}) - \frac{1}{\mathbf{k}}(1 - e^{-\mathbf{k}\alpha})\right)e^{-k[\gamma + (n-1)\alpha + (n-1)\beta]} \tag{6}$$

where b_n is the initial value of $[\mathrm{LR}]_n$ (see Appendix), $k = L_T k_f + k_f$, and $\mathbf{k} = k_r + k_p$.

S_n is written as a function of excitation period number, n, rather than as a function of time. Acquisition parameters α and β were preset for each experiment and recorded accurately to within millisecond resolution. However, the initial lag time, γ, was not as well defined experimentally as α and β because the precise time of solution exchange was not determined electronically; it is uncertain by less than ± 2.5 s. Equation 5 contains four unknown parameters, k_r, k_f, k_p, and Q. The total ligand concentration, L_T, is known for each experiment. The total receptor density, R_T, is set arbitrarily to 2×10^6 receptors/cell and is multiplied by the scaling factor Q.

The photobleaching correction for ligand debinding experiments was derived similarly. The debinding exposure scheme was the same as that for binding, except that the initial lag time, γ, was not important for debinding. The solution to the debinding reaction scheme was also obtained iteratively. The final equation for the measured signal S_n has the same form as Eq. 5, except that integrated [LR] during each exposure is

$$\int_0^{\alpha} [\mathrm{LR}]_n \, dt = \frac{[\mathrm{LR}]_0}{\mathbf{k}}(1 - e^{-\alpha \mathbf{k}})e^{-(n-1)(\alpha \mathbf{k} + \beta k_r)} \tag{7}$$

Three unknown parameters, k_r, k_p, and Q, are required to describe ligand debinding.

As the photobleaching constant k_p approaches 0, binding and debinding S_n's become the integrated forms of simple exponential functions. The derived binding and debinding equations can be extended to correct for the photobleaching effect in the two independent monovalent sites model by summing two independent binding or debinding equations.

Single-cell kinetics of f-EGF binding and debinding

The kinetics observed for single cells consistently showed a biphasic appearance, characterized by a fast binding/debinding phase followed by a slower binding/debinding phase. For example, f-EGF binding did not reach equilibrium during 80 min of binding (Fig. 7 *A*) in the presence of a low [f-EGF] (0.62 nM). The corresponding f-EGF debinding (Fig. 7 *B*), recorded from the same cell immediately after the binding experiment, did not reach the zero fluorescence level during the 70-min experiment. Similar characteristics in kinetics were also observed for binding experiments (Fig. 7 *C*) performed at 1.23 nM f-EGF and the corresponding debinding experiments (Fig. 7 *D*). Kinetic curves fitted to the data from both experiments showed an initial fast binding/debinding phase and a subsequent long-lasting slow binding/debinding phase. The rate constants returned from the fits are given in the figure legend. The slow kinetic phases in binding and debinding were not the result of nonspecific f-EGF binding to or debinding from cells/coverslips (see the nonspecific binding control experiment of Fig. 2). The biphasic appearance in the kinetic curves was therefore not an artifact of the experimental techniques.

Binding curves displaying different kinetic characteristics were observed for different cells of the same coverslip or different cells from different experiments using different [f-EGF]. Three examples of binding curves collected at three [f-EGF] are shown in Fig. 8. The rate constants used to generate the fits are given in the figure legend. At high [f-EGF] (6.15 nM), two types of binding curves were observed, biphasic curves with a slow upward trend (not shown) or biphasic curves with a slow downward trend (Fig. 8 *A*). At 1.23 nM (Fig. 7 *C*) and 2.46 nM (Fig. 8 *B*) [f-EGF], only biphasic binding curves with a slow upward trend were observed. At low [f-EGF] (0.62 nM), both biphasic binding curves with a slow upward trend (not shown) and monophasic binding curves (Fig. 8 *C*) were observed. All of the biphasic curves were modeled reasonably well by the two-site model (*thick lines*) but poorly modeled by the one-site model (*thin lines*). The monophasic curves observed at 0.62 nM f-EGF were modeled equally well by either model.

Considerable cell-to-cell variation in the f-EGF kinetic binding parameters was found in all experiments. Table 1 shows the results from fits to the two-site model for four cells from one coverslip exposed to 6.15 nM f-EGF. The forward and reverse rate constants are grouped together, corresponding to high- and low-affinity sites where the affinity constants are computed as the ratio of the fitted reverse and forward rate constants ($K = k_r/k_f$). The site exhibiting faster kinetic rate constants corresponds to the lower affinity constant. The fractions of sites that exhibit fast kinetics (i.e., the low-affinity site) are shown as f_{fast}. Also shown in the table are the relative numbers of receptors for each cell, normalized to the number of receptors on cell 1. These data demonstrate that there is considerable

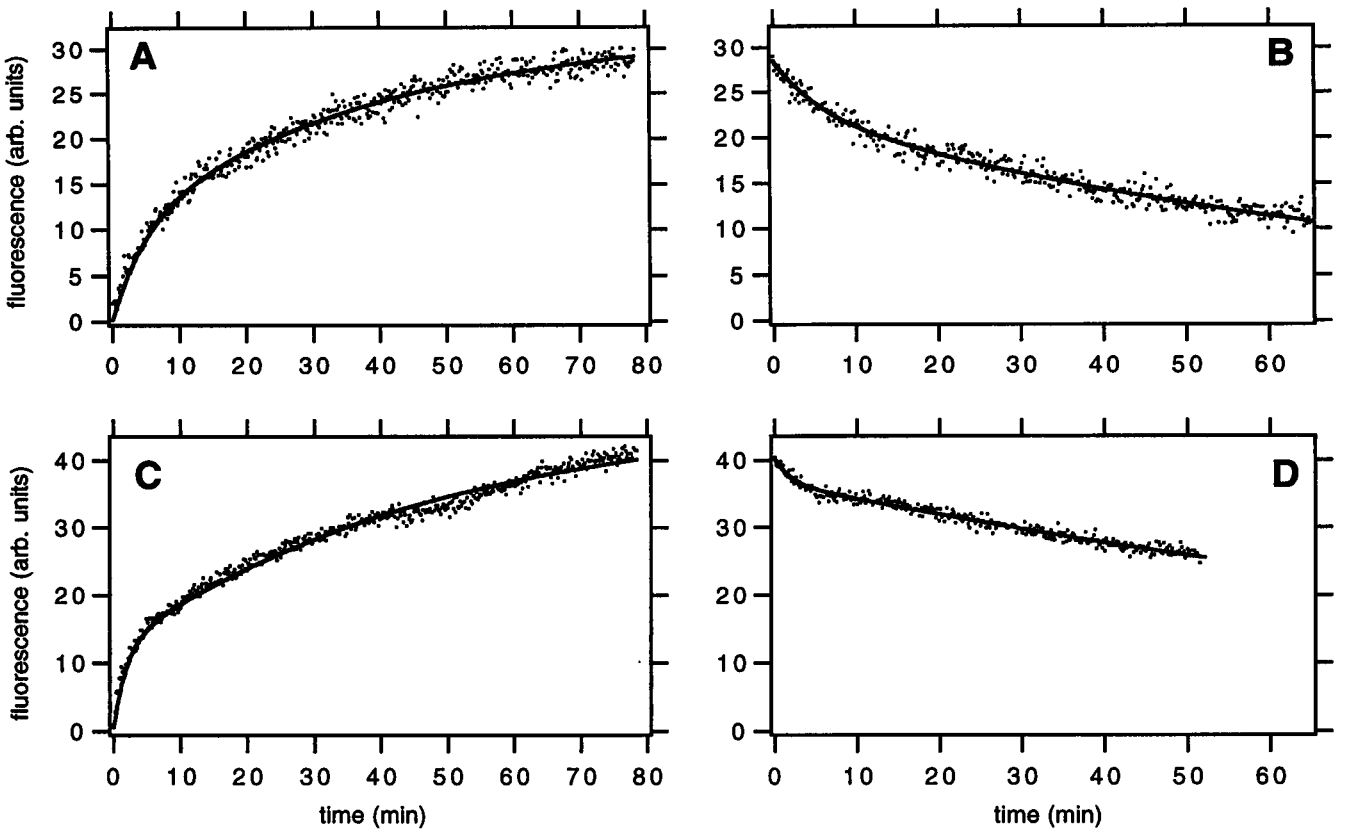

FIGURE 7 Binding and debinding of f-EGF on individual A431 cells. (*A*) Binding data (*dots*) for [f-EGF] = 0.62 nM were collected approximately every 10 s, using a 250-ms exposure time and curve-fit to the two independent monovalent site model (*line*). The parameter values of the two-site model used to generate the fitted curves were $k_r = 0.00019\ s^{-1}$, $k_p = 2 \times 10^{-5}\ s^{-1}$, $k_f = 0.00035\ s^{-1}\ nM^{-1}$, $Q = 0.00034$, $k'_r = 0.003\ s^{-1}$, $k'_p = 2 \times 10^{-5}\ s^{-1}$, $k'_f = 0.00042\ s^{-1}\ nM^{-1}$, and fraction of high-affinity receptors = 0.25. (*B*) Debinding of previously bound f-EGF was followed on the same cell as in *A*, immediately after removal of free f-EGF from the bathing solution using the same imaging parameters. The two-site model fit (*line*) produced the following parameters: $k_r = 0.003\ s^{-1}$, $k_p = 2 \times 10^{-5}\ s^{-1}$, $S(t = 0) = 114$, $k'_r = 0.00019\ s^{-1}$, $k'_p = 2 \times 10^{-5}\ s^{-1}$, and fraction of bound high-affinity receptors = 0.2. (*C*) Binding data (*dots*) were collected at 1.23 nM f-EGF, subject to the same imaging parameters as in *A*, and were curve-fit to the two independent monovalent site model (*line*). The parameter values of the two-site model used to generate the fitted curves (*lines*) were $k_r = 0.000115\ s^{-1}$, $k_p = 1.16 \times 10^{-5}\ s^{-1}$, $k_f = 0.000185\ s^{-1}\ nM^{-1}$, $Q = 0.00087$, $k'_r = 0.0084\ s^{-1}$, $k'_p = 1.9 \times 10^{-5}\ s^{-1}$, $k'_f = 0.00023\ s^{-1}\ nM^{-1}$, and fraction of high-affinity receptors = 0.12. (*D*) Debinding of previously bound f-EGF was followed on the same cell as in *C*, immediately after removal of free f-EGF from the bathing solution, using the same imaging parameters. The two-site model fit (*line*) produced the following parameters: $k_r = 0.0084\ s^{-1}$, $k_p = 1.16 \times 10^{-5}\ s^{-1}$, $S(t = 0) = 160.5$, $k'_r = 0.000115\ s^{-1}$, $k'_p = 1.16 \times 10^{-5}\ s^{-1}$, and fraction of bound high-affinity receptors = 0.087.

variation in apparent rate constants of f-EGF binding between cells and that the distribution between the numbers of high- and low-affinity receptors on A431 cells also shows a large variability from cell to cell.

Model simulations

Simulations of f-EGF binding to single cells were generated by applying the aforementioned models to kinetic constants obtained from population binding experiments reported in the literature (van Bergen en Henegouwen et al., 1989). Two independent receptor populations were assumed by these authors, who also measured ^{125}I-EGF debinding in the presence of 200 ng/ml EGF. Two dissociation rate constants were reported, one fast and one slow, of magnitudes $1.1 \times 10^{-3}\ s^{-1}$ and $3.5 \times 10^{-5}\ s^{-1}$, respectively. From steady-state Scatchard experiments, the high- and low-affinity dissociation constants are 0.7 nM and 8.5 nM, respectively. By

TABLE 1 Cell-to-cell variation of f-EGF binding parameters

Cell no.	Low-affinity site		High-affinity site		K_{high} (nM)	K_{low} (nM)	f_{fast}	Relative no. of receptors
	k_r (s^{-1})	k_f ($nM^{-1}\ s^{-1}$)	k_r (s^{-1})	k_f ($nM^{-1}\ s^{-1}$)				
1	1.4×10^{-4}	2.2×10^{-3}	5.0×10^{-6}	1.2×10^{-4}	0.04	0.06	0.38	1
2	1.8×10^{-3}	2.3×10^{-3}	9.9×10^{-6}	1.5×10^{-4}	0.07	0.8	0.28	1.1
3	1.5×10^{-4}	5.0×10^{-3}	8.1×10^{-5}	2.1×10^{-4}	0.03	0.4	0.28	0.68
4	1.1×10^{-4}	2.7×10^{-3}	6.5×10^{-5}	4.3×10^{-4}	0.04	0.2	0.47	1.2

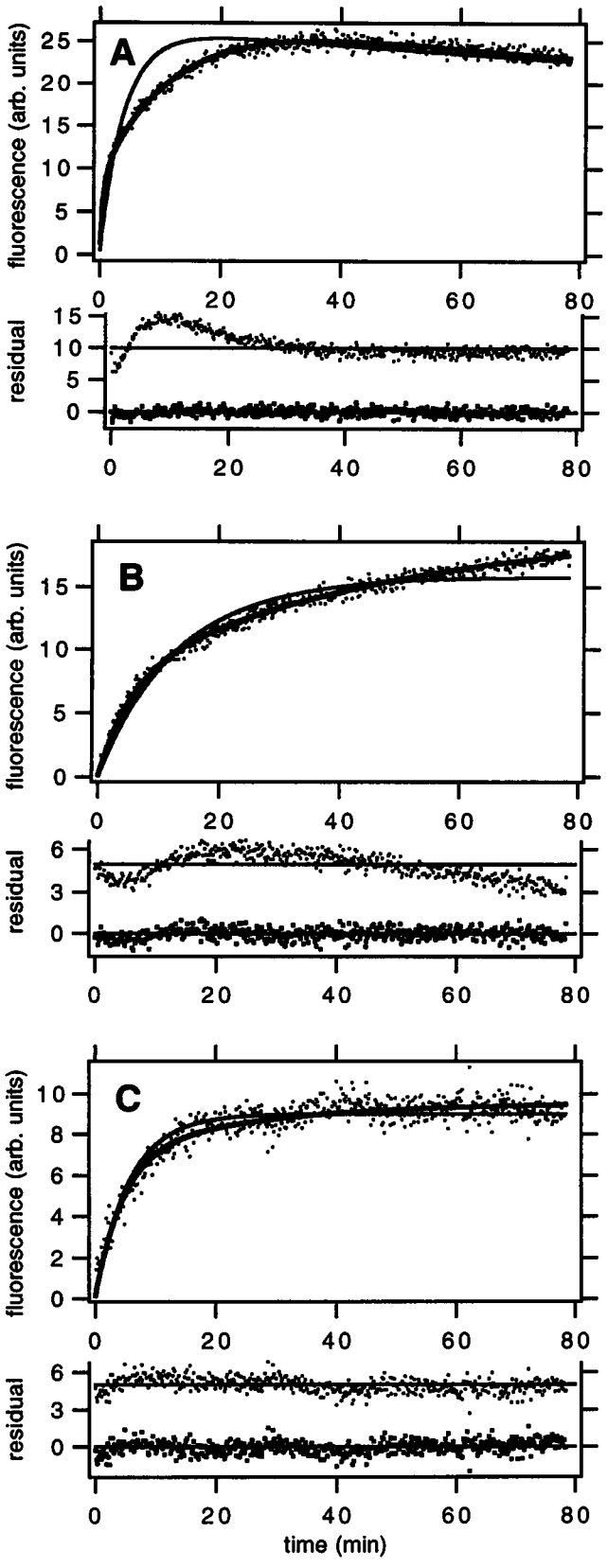

FIGURE 8 Binding data collected at different [f-EGF]. The data were collected at ~10-s intervals, using 500-ms exposure times. Thin lines are curves predicted by the one-site model. Thick lines are curves predicted by the two-site model. The corresponding residual plots (*dots*; residual plots for the one-site model are offset by 5 or 10 fluorescence units for clarity) are shown just below the binding data (*dots*). (*A*) Binding data collected at 6.15 nM f-EGF. The parameter values of the two-site model are k_r = 0.00015 s^{-1}, k_p = 0.00073 s^{-1}, k_f = 0.005 s^{-1} nM^{-1}, $Q = 3 \times 10^{-5}$, k'_r = 8.1 × 10^{-5} s^{-1}, k'_p = 0.0016 s^{-1}, k'_f = 0.00021 s^{-1} nM^{-1}, and fraction of high-affinity receptors = 0.28. The parameter values of the one-site model are $k_r = 1.5 \times 10^{-5}$ s^{-1}, k_p = 0.0007 s^{-1}, k_f = 0.00065 $s^{-1}nM^{-1}$, $Q = 2.65 \times 10^{-5}$. (*B*) Binding data collected at 2.46 nM f-EGF. The parameter values of the two-site model are $k_r = 8.65 \times 10^{-6}$ s^{-1}, k_p = 0.00023 s^{-1}, k_f = 0.0012 s^{-1} nM^{-1}, $Q = 3 \times 10^{-5}$, k'_r = 0.00011 s^{-1}, k'_p = 0.00051 s^{-1}, $k'_f = 7.98 \times 10^{-5}$ s^{-1} nM^{-1}, and fraction of high-affinity receptors = 0.25. The parameter values of the one-site model are $k_r = 1 \times 10^{-5}$ s^{-1}, $k_p = 1 \times 10^{-5}$ s^{-1}, k_f = 0.0005 s^{-1} nM^{-1}, $Q = 1.6 \times 10^{-5}$. (*C*) Binding data collected at 0.62 nM f-EGF. The parameter values of the two-site model are k_r = 0.00048 s^{-1}, k_p = 0.0029 s^{-1}, k_f = 0.005 s^{-1} nM^{-1}, $Q = 3.7 \times 10^{-5}$, k'_r = 0.000349 s^{-1}, k'_p = 0.0031 s^{-1}, k'_f = 0.00015 s^{-1} nM^{-1}, and the fraction of high-affinity receptors = 0.21. The parameter values of the one-site model are $k_r = 3.1 \times 10^{-5}$ s^{-1}, $k_p = 5 \times 10^{-6}$ s^{-1}, k_f = 0.0047 s^{-1} nM^{-1}, $Q = 9.1 \times 10^{-6}$.

assigning to the low-affinity receptor the fast reverse rate, two forward rate constants of the high- and low-affinity classes were calculated to be 5×10^{-5} s^{-1} nM^{-1} and 1.3×10^{-4} s^{-1} nM^{-1}, respectively. The measured fraction of receptors in the high-affinity state from their data was 4%, which was applied to the two-site model simulation here. Kinetic constants of low-affinity receptors were used for the one-site model simulations. Predicted binding and debinding curves at different [f-EGF] for both the one-site (*dashed lines*) and two-site (*solid lines*) models based on the above EGFR kinetic rate constants are shown in Fig. 9. The photobleaching rate for f-EGF bound to either a high-affinity or a low-affinity receptor was assumed to be the same and was assigned to be 0.0005 s^{-1}, a value in the range of those in the experiments reported here; the photobleaching rate was varied systematically, to examine its effect on the models (Fig. 10).

During the binding phase of the simulated experiments (Fig. 9, *top*), the two models produced similar curves at each [f-EGF]; however, one slight difference did exist between the simulations by the two models. The simulations of the two-site model showed a slight upward trend in binding even after 1 h of binding, whereas the simulations of the one-site model reached a plateau in binding in less than 1 h. Nevertheless, the difference between the two models with the assigned rate constants was small and was not likely to be detectably different in the presence of actual experimental noise. As a result, the simulations predicted monophasic binding curves, if both the models and the reported rate constants were accurate.

In the debinding phase of the simulated experiments (Fig. 9, *bottom*), the fluorescence levels decreased to close to zero in 1 h of debinding for both models at different [f-EGF]. Visually, there were no other particular characteristics associated with the debinding curves predicted by the two models, using the assigned rate constants. However, the reverse rates used in these simulations were obtained from population debinding experiments in the presence of excess

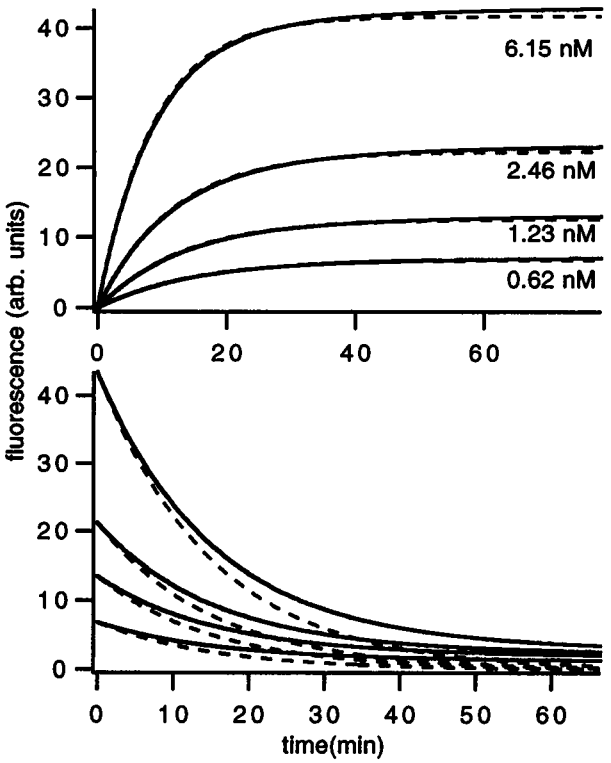

FIGURE 9 Model simulations. The binding and debinding kinetics of one-site (– – –) and two-site (——) models were simulated for four different [f-EGF], as indicated using the rate constants described in the text. The initial fluorescence levels for debinding simulations were set equal to the final fluorescence levels in the binding simulations.

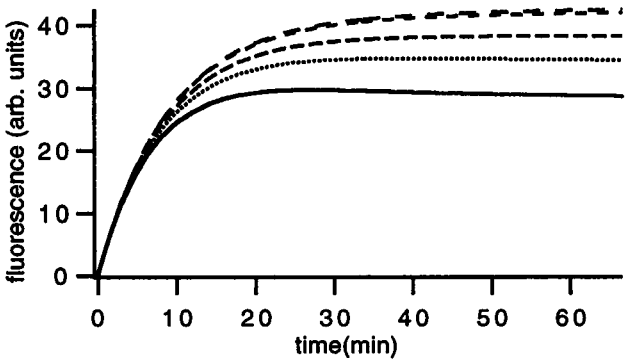

FIGURE 10 The effect of different f-EGF photobleaching rates on model simulations. The same parameters used for the two-site model simulations in Fig. 7 are applied here ([f-EGF] = 6.15 nM), except for the f-EGF photobleaching rate. This rate was assigned values of 0.0005 s^{-1}, 0.001 s^{-1} (*two closely spaced dashed lines, in descending order*), 0.005 s^{-1} (*dashed line*), 0.01 s^{-1} (*dotted line*), or 0.02 s^{-1} (*solid line*).

unlabeled EGF (200 ng/ml), and might have been faster than those obtained from the present debinding experiments performed in the absence of unlabeled EGF if EGF bound to EGFR by a diffusion-limited process. The high EGFR densities expressed by A431 cells have been reported to affect the kinetics of binding of EGF to these cells, possibly through diffusion-limited processes (Berkers et al., 1992; Wiley, 1988). One manifestation of a diffusion-limited process is that the effective rates of ligand-receptor dissociation become dependent on the extent of receptor occupancy (Bell, 1978; DeLisi and Wiegel, 1981); the addition of unlabeled EGF in dissociation experiments increases receptor occupancy by the binding of unlabeled EGF to free receptors, and therefore reduces the receptor densities available for the reassociation of free labeled EGF. As a result, the measured effective reverse rates are faster than those recorded in the absence of unlabeled EGF if the kinetic process is diffusion-limited.

The overall effect of f-EGF photobleaching was to drive the binding curves downward during a long experiment (>30 min; Fig. 9) and to drive the debinding curves toward a zero fluorescence level more rapidly (not shown). In the examples shown in Fig. 9, photobleaching rates below 0.001 s^{-1} show little effect on the simulated binding data, and even less effect if noise is included in the simulations (not shown); however, the downward trend becomes quite apparent when the photobleaching rate reaches ~0.02 s^{-1}.

Two of the three types of binding curves, monophasic, biphasic with a slow upward trend, and biphasic with a slow downward trend, observed in binding kinetics were not predicted by the simulations in Fig. 9, which all produced apparent monophasic binding in the range of [f-EGF] used for the experiments. The observed variations in f-EGF binding to different cells from the same coverslips or different experiments can be attributed to three possibilities: different f-EGF photobleaching rates between cells, cellular heterogeneity, or kinetic schemes that differ from the simple models used here. Different f-EGF photobleaching rates on different areas of the same field, caused by uneven illumination, can result in different binding curves in certain cases, as demonstrated by the simulations in Fig. 10; however, the severalfold differences in illumination intensity required to change the photobleaching rate are not found in the imaging system employed here. Different cells could exhibit different binding kinetics for a variety of reasons, e.g., different proportions of high-affinity receptors in the total cell receptor populations; different receptor densities, as in the case of diffusion-limited kinetics; and so on. Of course, the description of two static receptor populations used to describe the binding kinetics can simply be wrong, implying that a different model is required to correctly describe the observed kinetics.

DISCUSSION

Equilibrium or kinetic binding studies of ligand-receptor interactions on intact cells have previously been limited to assays incorporating thousands to millions of cells. Such assays, although sensitive and easy to perform, are intrinsically limited to the measurement of ensemble average values of receptor-binding site number and affinity. For the epidermal growth factor receptor and any other receptor that

demonstrates multiple affinity states, the analysis of data from large numbers of cells is ambiguous, in that individual cell heterogeneity or molecular heterogeneity could both provide valid interpretations of the data. The single-cell kinetic binding analysis presented here obviates this ambiguity and permits one to discern between cellular and molecular heterogeneity. Furthermore, the single-cell binding technique allows, in principle, the direct measurement of kinetic binding rates down to the optical resolution limit, i.e., at the dimension of plasma membrane domains.

Given the complexity of even the simple two-site binding model for the interaction of EGF and the EGFR, the data analysis methodology described above is most useful in eliminating models, as in the case of eliminating the one-site model, rather than validating a specific model. The results presented here suggest that the two-site model that incorporates independent EGFRs of two affinity states is consistent with all f-EGF single-cell binding data, whereas the one-site model fits poorly to the same data, except for a few cases at low [f-EGF] (0.65 nM). This indicates that the reported heterogeneity in receptor binding affinity based on bulk cell EGF binding assays exists at the single-cell level. Nevertheless, the simple two-site model is unlikely to be the correct model for the f-EGF binding events at the A431 cell surface, because interconversion between receptor affinity classes involving several different regulatory mechanisms, such as receptor dimerization (Schlessinger, 1988; Yarden and Schlessinger, 1987) and actin binding (van Belzen et al., 1991; van Bergen en Henegouwen et al., 1992), has been reported. Such interconversions require more kinetic steps in modeling and thus would intrinsically produce more complicated equations that predict single-cell EGF binding behavior. Given the fact that a simple two-site model requires eight parameters for full characterization and that such a model fits the observed data well, it seems unrealistic at this point to attempt to model more complex processes, because it is unlikely that the data would permit conclusive determination of their validity.

All experiments described here were carried out at 4°C, a temperature at which the internalization of ligand-bound EFGR is blocked in A431 cells (Miller et al., 1986). Thus the multiphasic f-EGF binding kinetics observed do not arise from internalization of ligand, but rather are due to the intrinsic ligand-receptor interactions on the cell surface.

It is not surprising that variations exist among cells in the number of total EGFR per cell and in the distribution between the high- and low-affinity binding classes of EGFR. Such variations should be the natural consequence of variable gene expression and posttranslational modification patterns, both of which depend on the environment in which a cell has grown. More surprising is the apparent variation in kinetic binding and debinding rates, as shown in Table 1 and Figs. 7 and 8. Such variation should not be present if the populations of high- and low-affinity EGFR are stable over time and if the EGF-EGFR binding interaction is due to a well-defined molecular structure adopted by the EGFR at each of its affinity states. One explanation for the variation in rate constants that derive from the binding data presented here is that the population of EGFR that is being sampled on each cell is nonstationary, that is, that transitions between apparent affinity states are occurring during the course of the f-EGF binding experiments. Such nonstationary behavior would clearly produce f-EGF binding data that are not properly modeled by the two-site model applied here. A second explanation is that the idea of two independent affinity states is not valid, and that other molecular interactions besides a direct change in the receptor-ligand interaction are responsible for the observed multiple kinetic rates and affinity states. One such interaction could involve variation in clustering of EGFR on the cell surface, such that some clusters present a much higher effective surface density than other clusters, with the higher density clusters exhibiting a greater degree of diffusion-limited ligand binding.

The derived kinetic parameters determined from the single-cell f-EGF binding data shown here depart considerably from bulk equilibrium binding data in the literature in two important regards. First, the fraction of receptors that are of the high-affinity class is much greater in the single-cell experiments than in equilibrium assays. This result would be consistent with the notion that a much larger number of EGFRs on a cell are in the high-affinity state before EGF binding, and that the cell responds to EGF stimulation by driving the conversion of high-affinity receptors to the low-affinity state, perhaps by a mechanism similar to that induced by phorbol ester treatment of A431 cells (Northwood and Davis, 1989). The rapid phase of f-EGF binding recorded by the technique described here thus contains a significant contribution of the state of the EGFR system before ligand application, and would therefore sample a larger fraction of high-affinity receptors if the above idea is valid. The second departure from bulk equilibrium binding data is in the apparent affinities of the high- and low-affinity receptor classes, particularly that of the low-affinity receptor. The values derived from the kinetic parameters from the fits described here are 2- to 10-fold lower than the values from bulk equilibrium binding data. Again, these departures could be due to the rapid sampling time employed in the present experiments, leading to a bias toward the state of the EGFR system that existed before ligand application. One should note that not all single-cell f-EGF binding affinities measured as described here are less than those in the literature; calculation of affinity constants based on the kinetic parameters given in the captions to Figs. 7 and 8 produces values for the high-affinity state that range from 0.01 nM to 0.6 nM, whereas for the low-affinity state the range is 0.4–37 nM. The results here suggest that single-cell, time-dynamic ligand binding assays produce data that complement bulk equilibrium binding data and that the single-cell assay may be useful in extending the study of ligand-receptor interactions to a finer resolution.

It is clear that quantitative analysis of ligand binding kinetics involving fluorescent ligands requires careful correction of fluorophore photobleaching during the course of

an experiment. The f-EGF photobleaching correction that is described here has two potential complicating factors. One is that f-EGF photobleaching may not be a first-order process. Photobleaching of a dye molecule is most often modeled as a first-order process; however, a recent study has demonstrated that such photochemistry is very sensitive to the microenvironment in which the reaction takes place (Song et al., 1995). Because it is difficult to measure the photobleaching process in the in vivo EGF/receptor system, it has not been possible to determine conclusively that only first-order kinetics are appropriate.

Another difficulty with f-EGF photobleaching correction for single-cell kinetic binding measurements is that the number of adjustable parameters for curve-fitting becomes large in any multiaffinity model (e.g., eight parameters for the two-site model). With such a large parameter space, it is difficult to locate the absolute minimum of a best fit in a least-squares fitting algorithm, and it is difficult to determine if the fitting parameters are correlated with each other. Curve-fitting of models to data should provide 1) parameter values for the models, 2) error estimates for the parameter values, and 3) a measurement of goodness of fit for the fit (Press et al., 1992). The noise in the single-cell binding data and the large number of parameters together allow one to find multiple sets of parameters that all produce reasonable fits to the data for a given criterion of goodness of fit (e.g., χ^2 minimization), making it difficult to find the best fit. A systematic survey of parameter space is therefore necessary to best approximate the best fit; such a survey becomes very computation-intensive as the number of parameters increases, and was not implemented for the present study. In addition to the problem of locating the absolutely best fit of a model to the data, uncertainty estimates for the fitted parameters also present a problem in cases in which the kinetic equations have low sensitivity to certain parameters. For example, the $L_T k_f$ term in $k = L_T k_f + k_r$ can be much larger than the k_r term, making k relatively insensitive to k_r. Similarly, the two terms on the left side of $\mathbf{k} = k_r + k_p$ can also differ by orders of magnitude, resulting in less sensitivity of the overall equations to one term or the other. Such low sensitivity for a parameter results in large uncertainty estimates for the parameter when the binding equations are fitted to real data.

One approach to resolving some of the difficulties in data fitting for a few specific cases is to perform both binding and debinding experiments on the same cells consecutively, and to first fit the debinding phase of the experiment, which generally has fewer adjustable parameters. Using the one-site model as an example, debinding data can be fit to obtain two kinetic variables, k_r and k_p. Subsequently, binding data from the same cell region can be fit by holding the two newly determined parameters, k_r and k_p, constant to obtain the third kinetic parameter, k_f. However, this approach only works well for simple models, because the number of parameters is still large for debinding kinetics in multiaffinity or other, more elaborate models. It also presumes that all rate constants in multiaffinity models do not vary with time, an assumption that must be evaluated for each experimental protocol.

Concentration-dependent quenching of f-EGF fluorescence on the cell surface could, in principle, artifactually alter the apparent f-EGF binding and debinding kinetics. Although a systematic study of concentration quenching of f-EGF on the cell surface was not performed in this study, comparison of data from debinding experiments in which the fluorescence of A431 cells preincubated with either f-EGF (3 nM) alone or f-EGF (1.85 nM) plus unlabeled EGF (1.33 nM) together did not suggest that f-EGF concentration quenching, if present, altered the measured ligand binding kinetics. After an initial preincubation, washing the cells with HBS to remove unbound f-EGF and unbound EGF produced identical rates of f-EGF debinding (not shown). This suggests that any enhancement of f-EGF fluorescence that might be occurring as the cell surface concentration decreases with debinding is not sufficiently large to alter the measured loss of f-EGF fluorescence due to true ligand debinding.

The data presented here are derived from the average ligand binding interactions over a large region of a single cell. As the data were recorded with a wide-field microscope, the f-EGF binding data reflect the molecular properties of the apical side of the A431 cells studied. Receptor lateral mobility at the cell surface has been assumed not to interfere with the measurement of averaged fluorescence intensity obtained from the whole top surface of a cell. Specifically, possible receptor aggregation and diffusion into and out of a region were assumed not to change the region's total number of receptors over the course of an experiment. Measurements of EGFR lateral diffusion coefficients on A431 cell membranes yield values in the range of $2–4 \times 10^{-10}$ cm^2/s at temperatures near 5°C for the fraction of receptors that are mobile (Rees et al., 1984; Hillman and Schlessinger, 1982). The data in Figs. 7–9 show that the most rapid kinetic phase of EGF binding to A431 cells is ligand concentration dependent; at 6 nM [EGF] the rapid phase lasts ~1 min, whereas the slower phase has a characteristic time of 15–20 min. Thus laterally mobile EGFR could move over characteristic distances of ~3 μm during the fast phase and ~12 μm during the slow phase. Both of these distances were calculated assuming unrestricted movement of receptors in the plasma membrane. If, indeed, EGFR are free to diffuse across the entire A431 cell plasma membrane, these numbers demonstrate that only the rapid kinetic phase of the f-EGF binding curves would sample local (~3 μm dimension) regions of the membrane, whereas the slower phase data would sample nearly all mobile EGFR, as the diffusion distance is comparable to the size of a cell. Results presented here suggest that both rapid and slow kinetic f-EGF binding vary from cell to cell. This is consistent with the idea that EGFR movements are restricted to domains on the cell surface and that the kinetic ligand-binding properties of domain-restricted EGFR are different between domains. It has recently been demonstrated that EGFR are concentrated in the

caveolar membrane fraction of human fibroblasts (Smart et al., 1995) and Rat-1 fibroblast cells (Mineo et al., 1996). It may be that interaction of EGFR with caveolae and potential immobilization of EGFR within these membrane organelles contribute to both the measured differential ligand-binding properties of EGFRs on different A431 cells and potentially differential signaling capacities of these localized receptors. It is interesting to note that actin concentration is also elevated in caveolar membrane preparations (Lisanti et al., 1994) and that the EGFR contains an actin-binding sequence in its cytoplasmic domain (den Hartigh et al., 1992). These facts, in combination with our measurements, are consistent with the idea that caveolae-associated actin restrains EGFRs within these cell surface structures and that such restraint modulates EGFR ligand binding affinity. Other experiments will be necessary to test this hypothesis.

Several factors in modeling EGF/receptor interactions have not been studied in the present paper. For example, a 1:1 molar ratio stoichiometry of EGF to EGFR binding has been reported by Weber, Bertics, and Gill (Weber et al., 1984a); however, other laboratories (Lemmon and Schlessinger, 1994; Stokes et al., 1994) have suggested that 1:2 (EGF to EGFR) binding stoichiometry is possible. Two recent reports present data showing that EGFR dimers can bind one or two EGF ligands such that four separate EGFR-EGF species can be present (i.e., R, LR, LR_2, and L_2R_2) (Sherrill and Kyte, 1996; Lemmon et al., 1997). In the former case, holoreceptors solubilized by Triton X-100 were employed, whereas in the latter the soluble extracellular domain of the receptor was studied. Because the effect of EGFR dimerization on intact cells has yet to be completely characterized for its effect on EGF binding, in this report only a simpler model of the interaction of EGF with the EGFR has been employed. Future work may be able to address this question.

Despite the simplicity of the models tested and the possible problems in data analysis, the two-site model fits reasonably well all data collected to date. This result is consistent with the existence of at least two affinity classes of receptors that are present simultaneously at the single-cell level. The model assumes that the two populations of receptors are static, which might not be the case on the cell surface; interconversion between receptor affinity classes can take place via oligomerization, posttranslational modification, or complexation with regulatory factors. The sensitivity of the single-cell binding assay to differences between these models has not been systematically analyzed and is an important point for future analysis.

APPENDIX

The solution for the one-monovalent-site model during a binding experiment is given below. A similar method is used to obtain the solutions for debinding experiments and for the two-independent-monovalent-site model.

Assume that $[L] \cong L_T \cong [L] + [L^*]$, and note that $d[R]/dt$ is independent of k_p. Then [R] can be solved explicitly for each segment.

Defining $k = L_T k_f + k_r$ and $\mathbf{k} = k_r + k_p$, the differential equations for binding are

$$\frac{d[LR]}{dt} + k_r[LR] = L_T k_f[R] \qquad \text{during initial lag period } (\gamma) \tag{A.1}$$

$$\frac{d[LR]}{dt} + \mathbf{k}[LR] = L_T k_f[R] \qquad \text{during excitation pulse } (\alpha) \tag{A.2}$$

$$\frac{d[LR]}{dt} + k_r[LR] = L_T k_f[R] \qquad \text{between pulses } (\beta). \tag{A.3}$$

For the initial lag time, t varies from 0 to γ:

$$[LR]_\gamma(t) = \frac{L_T R_T k_f}{k}(1 - e^{-kt}) \tag{A.4}$$

During pulse 1, t varies from 0 to α, with $[LR]_1(0) = [LR]_\gamma(\gamma)$:

$$[LR]_1(t) = [LR]_\gamma(\gamma)e^{-\mathbf{k}t} + \frac{L_T R_T k_f}{k}\left[\frac{k_r}{\mathbf{k}}(1 - e^{-\mathbf{k}t}) + (e^{-kt} - e^{-\mathbf{k}t})\frac{L_T k_f}{\mathbf{k} - k}e^{-k\gamma}\right] \tag{A.5}$$

Between pulses 1 and 2, t varies from 0 to β, with $[LR]'_1(0) = [LR]_1(\alpha)$:

$$[LR]'_1(t) = [LR]_1(\alpha)e^{-k_r t} + \frac{L_T R_T k_f}{k}[1 - e^{-k_r t} + (e^{-k_r t} - e^{-kt})e^{-k(\gamma+n\alpha)}] \tag{A.6}$$

During pulse 2, t varies from 0 to α, with $[LR]_2(0) = [LR]'_1(\beta)$:

$$[LR]_2(t) = [LR]'_1(\beta)e^{-\mathbf{k}t} + \frac{L_T R_T k_f}{k}\left[\frac{k_r}{\mathbf{k}}(1 - e^{-\mathbf{k}t}) + (e^{-kt} - e^{-\mathbf{k}t})\frac{L_T k_f}{\mathbf{k} - k}e^{-k(\gamma+\alpha+\beta)}\right] \tag{A.7}$$

Similarly, during any pulse n, t varies from 0 to α, with initial [LR] equal to that at the end of the preceding interval:

$$LR]_n = b_n e^{-\mathbf{k}t} + \frac{L_T R_T k_f}{k} \cdot \left[\frac{k_r}{\mathbf{k}}(1 - e^{-\mathbf{k}t}) + (e^{-kt} - e^{-\mathbf{k}t})\frac{L_T k_f}{\mathbf{k} - k}e^{-k[\gamma+(n-1)\alpha+(n-1)\beta]}\right] \tag{A.8}$$

where

$$b_1 = \frac{L_T R_T k_f}{k}(1 - e - k_\gamma)$$

$$b_n = [LR]'_{n-1}(\beta), \qquad n > 1$$

The signal, S_n, detected by the CCD camera, is the integrated signal during each excitation pulse. The final equation for the measured signal S_n has the following form:

$$S_n = Q\int_0^\alpha [LR]_n\, dt \tag{A.9}$$

where Q is a scaling factor and

$$\int_0^{\alpha} [\mathrm{LR}]_n \, dt = \left(\frac{b_n}{\mathbf{k}} - \frac{L_T R_T k_f k_r}{\mathbf{k}^2 k}\right)(1 - e^{-\mathbf{k}\alpha}) + \frac{L_T R_T k_f k_r}{\mathbf{k} k}\alpha \tag{A.10}$$

$$+ \frac{L_T^2 R_T k_f^2}{k(\mathbf{k} - k)}\left(\frac{1}{k}(1 - e^{-k\alpha}) - \frac{1}{\mathbf{k}}(1 - e^{-\mathbf{k}\alpha})\right)e^{-k[\gamma + (n-1)\alpha + (n-1)\beta]}$$

We thank R. M. Weis, N. Layzer, and M. Holbrook for helpful discussions and David Tirrell for numerous suggestions and financial support.

This work is supported by grant MCB-9304393 from the National Science Foundation, by grant FRA-437 from the American Cancer Society, and by the NSF Materials Research Science and Engineering Center at the University of Massachusetts, Amherst.

REFERENCES

Bell, G. I. 1978. Models for the specific adhesion of cells to cells. *Science.* 200:618–627.

Bellot, F., W. Moolenaar, R. Kris, B. Mirakhur, I. Verlaan, A. Ullrich, J. Schlessinger, and S. Felder. 1990. High-affinity epidermal growth factor binding is specifically reduced by a monoclonal antibody, and appears necessary for early responses. *J. Cell Biol.* 110:491–502.

Berkers, J. A. M., P. M. P. van Bergen en Henegouwen, and J. Boonstra. 1992. The effect of receptor density and cell shape on epidermal growth factor binding. *J. Recept. Res.* 12:71–100.

Boonstra, J., P. Rijken, B. Humbel, F. Cremers, A. Verkleij, and P. van Bergen en Henegouwen. 1995. The epidermal growth factor. *Cell Biol. Int.* 19:413–429.

Carpenter, G. 1987. Receptors for epidermal growth factor and other polypeptide mitogens. *Annu. Rev. Biochem.* 56:881–914.

Carpenter, G., and S. Cohen. 1979. Epidermal growth factor. *Annu. Rev. Biochem.* 48:193–216.

Carpenter, G., and S. Cohen. 1981. EGF: receptor interactions and the stimulation of cell growth. *In* Receptors and Recognition. R. J. Lefkowitz, editor. Chapman and Hall, London. 41–66.

Carpenter, G., and S. Cohen. 1990. Epidermal growth factor. *J. Biol. Chem.* 265:7709–7712.

Carraway, K. L., III, and R. A. Cerione. 1991. Comparison of epidermal growth factor (EGF) receptor-receptor interactions in intact A431 cells and isolated plasma membranes. *J. Biol. Chem.* 266:8899–8906.

Chatelier, R. C., R. G. Ashcroft, C. J. Lloyd, E. C. Nice, R. H. Whitehead, W. H. Sawyer, and A. W. Burgess. 1986. Binding of fluoresceinated epidermal growth factor to A431 cell sub-populations studied using a model-independent analysis of flow cytometric fluorescence data. *EMBO J.* 5:1181–1186.

Cheyette, T. E., and D. J. Gross. 1991. Epidermal growth factor-stimulated calcium ion transients in individual A431 cells: initiation kinetics and ligand concentration dependence. *Cell Regul.* 2:827–840.

Chinkers, M., J. A. McKanna, and S. Cohen. 1979. Rapid induction of morphological changes in human carcinoma cells A-431 by epidermal growth factor. *J. Cell Biol.* 83:260–265.

Chinkers, M., J. A. McKanna, and S. Cohen. 1981. Rapid rounding of human epidermoid carcinoma cells A-431 induced by epidermal growth factor. *J. Cell Biol.* 88:422–429.

Cummings, R. D., A. M. Soderquist, and G. Carpenter. 1985. The oligosaccharide moieties of the epidermal growth factor receptor in A-431 cells. *J. Biol. Chem.* 260:11944–11952.

Davis, R. J., N. Gironès, and M. Faucher. 1988. Two alternative mechanisms control the interconversion of functional states of the epidermal growth factor receptor. *J. Biol. Chem.* 263:5373–5379.

Defize, L. H. K., J. Boonstra, J. Meisenhelder, W. Kruijer, L. G. J. Tertoolen, B. C. Tilly, T. Hunter, P. M. P. van Bergen en Henegouwen, W. H. Moolenaar, and S. W. de Laat. 1989. Signal transduction by epidermal growth factor occurs through the subclass of high affinity receptors. *J. Cell Biol.* 109:2495–2507.

DeLisi, C., and F. W. Wiegel. 1981. Effect of nonspecific forces and finite receptor number on rate constants of ligand-cell bound-receptor interactions. *Proc. Natl. Acad. Sci. USA.* 78:5569–5572.

den Hartigh, J. C., P. M. P. van Bergen en Henegouwen, A. J. Verkleij, and J. Boonstra. 1992. The EGF receptor is an actin-binding protein. *J. Cell Biol.* 119:349–355.

Fabricant, R. N., J. E. D. Larco, and G. J. Todaro. 1977. Nerve growth factor receptors on human melanoma cells in culture. *Proc. Natl. Acad. Sci. USA.* 74:565–569.

Gadella, T. W. J., Jr., and T. M. Jovin. 1995. Oligomerization of epidermal growth factor receptors on A431 cells studied by time-resolved fluorescence imaging microscopy. A stereochemical model for tyrosine kinase receptor activation. *J. Cell Biol.* 129:1543–1558.

Giard, D. J., S. A. Aaronson, G. J. Todaro, P. Arnstein, J. H. Kersey, H. Dosik, and W. P. Parks. 1973. In vitro cultivation of human tumors: establishment of cell lines derived from a series of solid tumors. *J. Natl. Cancer Inst.* 51:1417–1423.

Gregoriou, M., and A. R. Rees. 1984. Properties of a monoclonal antibody to epidermal growth factor receptor with implications for the mechanism of action of EGF. *EMBO J.* 3:929–937.

Haigler, H., J. F. Ash, S. J. Singer, and S. Cohen. 1978. Visualization by fluorescence of the binding and internalization of epidermal growth factor in human carcinoma cells A-431. *Proc. Natl. Acad. Sci. USA.* 75:3317–3321.

Haigler, H. T., J. A. McKanna, and S. Cohen. 1979. Direct visualization of the binding and internalization of a ferritin conjugate of epidermal growth factor in human carcinoma cells A-431. *J. Cell Biol.* 81:382–395.

Hillman, G. M., and J. Schlessinger. 1982. Lateral diffusion of epidermal growth factor complexed to its cell surface receptors does not account for the thermal sensitivity of patch formation and endocytosis. *Biochemistry.* 21:1667–1672.

Lax, I., F. Bellot, R. Howk, A. Ullrich, D. Givol, and J. Schlessinger. 1989. Functional analysis of the ligand binding site of EGF-receptor utilizing chimeric chicken/human receptor molecules. *EMBO J.* 8:421–427.

Lax, I., W. H. Burgess, F. Bellot, A. Ullrich, J. Schlessinger, and D. Givol. 1988. Localization of a major receptor-binding domain for epidermal growth factor by affinity labeling. *Mol. Cell. Biol.* 8:1831–1834.

Lemmon, M. A., Z. Bu, J. E. Ladbury, M. Zhou, D. Pinchasi, I. Lax, D. M. Engelman, and J. Schelssinger. 1997. Two EGF molecules contribute additively to stabilization of the EGFR dimer. *EMBO J.* 16:281–294.

Lemmon, M. A., and J. Schlessinger. 1994. Regulation of signal transduction and signal diversity by receptor oligomerization. *Trends Biochem. Sci.* 19:459–463.

Linderman, J. J., L. J. Harris, L. L. Slakey, and D. J. Gross. 1990. Charge-coupled device imaging of rapid calcium transients in cultured arterial smooth muscle cell. *Cell Calcium.* 11:131–144.

Lisanti, M. P., P. E. Scherer, J. Vidugiriene, Z. L. Tang, A. Hermanowski-Vosatka, Y.-H. Tu, R. F. Cook, and M. Sargiacomo. 1994. Characterization of caveolin-rich membrane domains isolated from an endothelial-rich source: implications for human disease. *J. Cell Biol.* 126:111–126.

Masui, H., L. Castro, and J. Mendelsohn. 1993. Consumption of EGF by A431 cells: evidence for receptor recycling. *J. Cell. Biol.* 120:85–93.

Mayes, E. L. V., and M. D. Waterfield. 1984. Biosynthesis of the epidermal growth factor receptor in A431 cells. *EMBO J.* 3:531–537.

McKanna, J. A., H. T. Haigler, and S. Cohen. 1979. Hormone receptor topology and dynamics: morphological analysis using ferritin-labeled epidermal growth factor. *Proc. Natl. Acad. Sci. USA.* 76:5689–5693.

Miller, K., J. Beardmore, H. Kantey, J. Schlessinger, and C. R. Hopkins. 1986. Localization of the epidermal growth factor (EGF) receptor within the endosome of EGF-stimulated epidermal carcinoma (A431) cells. *J. Cell Biol.* 102:500–509.

Mineo, C., G. L. James, E. J. Smart, and R. G. W. Anderson. 1996. Localization of epidermal growth factor-stimulated Ras/Raf-1 interaction to caveolae membrane. *J. Biol. Chem.* 271:11930–11935.

Northwood, I. C., and R. J. Davis. 1989. Protein kinase C inhibition of the epidermal growth factor tyrosine protein kinase activity is independent of the oligomeric state of the receptor. *J. Biol. Chem.* 264:5746–5750.

Press, W. H., B. P. Flannery, S. A. Teukolsky, and W. T. Vetterling. 1992. Numerical Recipes: The Art of Scientific Computing. Cambridge University Press, Cambridge, England.

Rees, A. J., M. Gregoriou, P. Johnson, and P. B. Garland. 1984. High affinity epidermal growth factor receptors on the surface of A431 cells have restricted lateral diffusion. *EMBO J.* 3:1843–1847.

Savage, C. R., Jr., T. Inagami, and S. Cohen. 1972. The primary structure of epidermal growth factor. *J. Biol. Chem.* 247:7612–7621.

Schlessinger, J. 1986. Allosteric regulation of the epidermal growth factor receptor kinase. *J. Cell Biol.* 103:2067–2072.

Schlessinger, J. 1988. Signal transduction by allosteric receptor oligomerization. *Trends Biochem. Sci.* 13:443–447.

Sherrill, J. M., and J. Kyte. 1996. Activation of epidermal growth factor receptor by epidermal growth factor. *Biochemistry.* 35:5705–5718.

Shimizu, N., and I. Kondo. 1982. Hyperproduction of EGF receptors in human A431 cells is regulated by a translocation chromosome, t(7; 11)(p22;q23). *Cytogenet. Cell Genet.* 32:316.

Slieker, L. J., and M. D. Lane. 1985. Post-translational processing of the epidermal growth factor receptor: glycosylation-dependent acquisition of ligand-binding capacity. *J. Biol. Chem.* 260:687–690.

Smart, E. J., Y.-s. Ying, C. Mineo, and R. G. W. Anderson. 1995. A detergent-free method for purifying caveolae membrane from tissue culture cells. *Proc. Natl. Acad. Sci. USA.* 92:10104–10108.

Song, L., E. J. Hennink, I. T. Young, and H. J. Tanke. 1995. Photobleaching kinetics of fluorescence in quantitative fluorescence microscopy. *Biophys. J.* 68:2588–2600.

Stokes, A. F., C. A. Guyer, K. L. Merritt, R. L. Woltjer, and J. V. Staros. 1994. A bifunctionally modified mutant EGF for probing the EGF binding site of the EGF receptor. *Protein Sci.* 3:128.

Taylor, J. M., W. M. Mitchell, and S. Cohen. 1972. Epidermal growth factor: physical and chemical properties. *J. Biol. Chem.* 247:5928–5934.

Tomoda, H., Y. Kishimoto, and Y. C. Lee. 1989. Temperature effect on endocytosis and exocytosis by rabbit alveolar macrophages. *J. Biol. Chem.* 264:15445–15450.

Ullrich, A., L. Coussens, J. S. Hayflick, T. J. Dull, A. Gray, A. W. Tam, J. Lee, Y. Yarden, T. A. Libermann, J. Schlessinger, J. Downward, E. L. V. Mayes, N. Whittle, M. D. Waterfield, and P. H. Seeburg. 1984. Human epidermal growth factor receptor cDNA sequence and aberrant expression of the amplified gene in A431 epidermoid carcinoma cells. *Nature.* 309:418–425.

van Belzen, N., P. J. Rijken, A. J. Verkleij, and J. Boonstra. 1991. Sulfhydryl reagents alter epidermal growth factor receptor affinity and association with the cytoskeleton. *J. Recept. Res.* 11:919–940.

van Bergen en Henegouwen, P. M. P., L. H. K. Defize, J. de Kroon, H. van Damme, A. J. Verkleij, and J. Boonstra. 1989. Ligand-induced association of epidermal growth factor receptor to the cytoskeleton of A431 cells. *J. Cell. Biochem.* 39:455–465.

van Bergen en Henegouwen, P. M. P., J. C. den Hartigh, P. Romeyn, A. J. Verkleij, and J. Boonstra. 1992. The epidermal growth factor receptor is associated with actin filaments. *Exp. Cell Res.* 199:90–97.

Weber, W., P. J. Bertics, and G. N. Gill. 1984a. Immunoaffinity purification of the epidermal growth factor receptor. *J. Biol. Chem.* 259: 14631–14636.

Weber, W., G. N. Gill, and J. Spiess. 1984b. Production of an epidermal growth factor receptor-related protein. *Science.* 224:294–297.

Weigel, P. H., and J. A. Oka. 1981. Temperature dependence of endocytosis mediated by the asialoglycoprotein receptor in isolated rat hepatocytes. *J. Biol. Chem.* 256:2615–2617.

Wiley, H. S. 1988. Anomalous binding of epidermal growth factor to A431 cells is due to the effect of high receptor densities and a saturable endocytic system. *J. Cell Biol.* 107:801–810.

Wrann, M. M., and C. F. Fox. 1979. Identification of epidermal growth factor receptors in a hyperproducing human epidermoid carcinoma cell line. *J. Biol. Chem.* 254:8083–8086.

Yarden, Y., and J. Schlessinger. 1987. Self-phosphorylation of epidermal growth factor receptor: evidence for a model of intermolecular allosteric activation. *Biochemistry.* 26:1434–1442.